Polymer Testing 129 (2023) 108286

Contents lists available at ScienceDirect

Polymer Testing

journal homepage: www.elsevier.com/locate/polytest

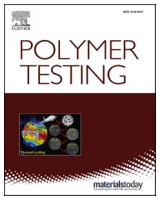

Methodology for the mechanical characterisation of hyperelastic adhesives. Experimental validation on joints of different thicknesses

F.J. Simón-Portillo [a,*], D. Abellán-López [a], F. Arán [b], L.F.M. da Silva [c], M. Sánchez-Lozano [a]

[a] Department of Mechanical and Energy Engineering, Miguel Hernandez University of Elche, 03202, Spain
[b] Footwear Technological Institute INESCOP, Elda, 03600, Alicante, Spain
[c] Department of Mechanical Engineering, Faculty of Engineering, University of Porto, Porto, 4200-465, Portugal

ARTICLE INFO

Keywords:
Finite element
Hyperelastic models
Characterisation
Flexible adhesives
Polyurethane

ABSTRACT

This work focuses on the mechanical characterisation of adhesives with hyperelastic behaviour and on the determination of the behavioural laws that best represent it, in order to introduce them in simulation models. First, a test plan is carried out on simple specimens: uniaxial and planar configuration. These are designed to measure the non-linear behaviour of adhesives in both tensile and pure shear. Unlike the uniaxial specimen, which is governed by a test standard (UNE-ISO 37) that defines its geometry, the planar specimen does not have a standard that defines its dimensions. Therefore, in this research it is proposed to carry out tests with specimens of different width-length sizes to evaluate how these dimensions affect the stress-strain curves.

For mechanical characterisation, finite element programs provide the tool to evaluate the predicted behaviour of a hyperelastic material from the experimental results, displaying in the same graph the degree of approximation obtained for the results of each test (Dumbbell and planar) with different hyperelastic models, allowing us to select the hyperelastic model that best fits the experimental data.

The Mooney-Rivlin model was found to be the best fitting model and therefore the most appropriate to describe the behaviour of hyperelastic adhesives used in this study. To conclude this study, the obtained law was validated by comparing the results of tests carried out on single lap joint (SLJ) specimens of different thickness.

1. Introduction

In recent years, the use of flexible adhesives for structural bonding applications has increased significantly. These adhesives are able to withstand large deformations without damage, making them ideal for applications where flexibility and strength are required. These bonding techniques are increasingly being used in the aerospace, automotive, marine and other industries [1–9].

In order to ensure the proper functioning of adhesive bonds, it is essential to study and optimise the bond. The use of Finite Element Models (FEM) can help [10–12]. For FEM modelling, it is essential to carry out a precise mechanical characterisation of the material. This entails defining and validating the behavioural laws of the adhesive used in these joints [9,13,14].

The adhesive considered for this research is a one-component polyurethane (PUR), the SikaFlex 252. It is used in the manufacture of car bodies, vehicles, as well as in the nautical industry, providing a strong and flexible bond, presenting a low elastic modulus. It also has good resistance to moisture and weathering [15,16]. This type of adhesive cures by reaction with moisture to form high performance elastomers. It exhibits non-linear elastic behaviour that can be described by hyper-elastic material constitutive models [17]. These types of models can describe the large deformation levels that these adhesives reach before failure. The constitutive models of hyperelastic materials are based on complex mathematical expressions based on the theory of large deformations [18,19]. In order to define the input requirements of the models, various tests may be required to identify the constitutive parameters of the material [20–26].

To improve the model fit of a hyperelastic material, it is advisable to follow a number of guidelines [27]. For example, obtaining test data for the deformation modes that are likely to occur in the final joint simulation. It is also important to include data from the planar test, which measures shear behaviour, and to provide more data on the strain magnitudes to which you expect the material to be subjected during the

* Corresponding author.
E-mail addresses: f.simon@umh.es (F.J. Simón-Portillo), dabellan@umh.es (D. Abellán-López), aran@inescop.es (F. Arán), lucas@fe.up.pt (L.F.M. da Silva), msanchez@umh.es (M. Sánchez-Lozano).

https://doi.org/10.1016/j.polymertesting.2023.108286
Received 10 August 2023; Received in revised form 17 October 2023; Accepted 23 November 2023
Available online 29 November 2023

simulation.

This research focuses on the characterisation of a flexible polyurethane adhesive and the adjustment of the model, based on test data from dumbbell-shaped (traction) and planar specimens (shear). Since there is no standard that establishes the test dimensions for the characterisation of planar specimens, in a first phase, tests of different dimensions have been carried out to study the influence of these dimensions on the behaviour curves.

The stress-strain curves for different hyperelastic models were then obtained from the tests of the different planar and dumbbell specimen geometries. The models that gave a better fit were selected by comparing the stress-strain curves obtained with those of the tests. Once the hyperelastic models were selected, the geometry of the planar specimen was chosen to best fit the behavioural laws of the adhesive. For this purpose, simulations of the SLJ specimen with 3 mm of adhesive thickness were carried out with the different models considered.

Once the hyperelastic model has been fitted as described in this article, it should be possible to use it to simulate the behaviour of different joint configurations. To confirm and validate the chosen material model, SLJ joints with different adhesive thicknesses were modelled computationally and the results compared with those obtained experimentally.

2. Methodology

2.1. Tests with planar specimen

To obtain the constants of the 1st and 2nd order hyperelastic models, stress-strain curves in two different loading configurations are required [28,29]. Uniaxial tensile test with dumbbell specimens and planar test, also known as "pure shear", were chosen. It is highly recommended to include the latter test in the characterisation of hyperelastic materials in order to take into account the shear behaviour of the material.

The planar specimens used in this study consist of thin sheets of adhesive subjected to tensile stress. As mentioned above, there are no standard dimensions for the planar specimen, and for this reason specimens of different dimensions will be tested, in order to compare the results obtained and choose the one that leads to the best fit. The specimens were fabricated from 200 × 130 mm adhesive sheets of the appropriate thickness and then cut to the dimensions given in Table 1 (Fig. 1). All specimens were cured in a controlled room at 23 ± 3 °C and 50 ± 5 % humidity, following the specifications of adhesive manufacturer. However, in order to ensure that the adhesive was fully cured, periodic hardness measurements of the adhesive sheets were taken (Durotech, Model M202). It was observed that from day 15 onwards these measurements remained constant, indicating full curing. Before die-cutting the specimens, a visual inspection was carried out to detect any internal defects in the adhesive sheets. The inspection method consisted of exposing the sheet to an intense beam of light, as described in Fig. 2 a), and photographing it to detect air bubbles trapped inside the adhesive and samples rejected if necessary (Fig. 2 b). It should be noted that no cavitation effects were observed, neither during these material

Table 1
Planar shear test dimensions (mm).

Nº	Width	Total Length	Effective length	Thickness
1	50	60	30	3
2	50	90	50	3
3	100	60	30	3
4	100	90	50	3
5	100	120	80	3
6	150	60	30	3
7	150	90	50	3
8	150	120	80	3
9	150	90	45	2
10	200	90	55	3

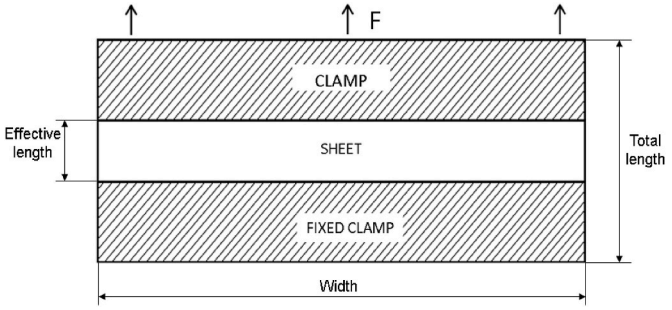

Fig. 1. Planar shear test geometry.

characterisation tests, nor in the joint specimen tests described below. In any case, the working range of interest for characterization is far from the fracture limits, where such an effect could be of greater importance [30].

Fig. 3 b) shows the clamps used for the test, which are made of 17mm thick birch plywood. Two steel plates help to distribute the pressure of the connecting bolts. The wood used has a stiffness 18 times greater than the adhesive to be tested, and it is verified that the tooling does not undergo any appreciable deformation during the test that could influence the result. In addition, double-sided tape is placed between the wood and the adhesive sheet to ensure that the adhesive does not slip during the test.

Tests on the planar specimens were performed using a universal testing machine equipped with a 20 kN load cell (Microtest) at a controlled displacement rate of 150 mm/min. This speed is somewhat lower than that established in ISO 37:2005 for the uniaxial tensile test (200 mm/min). However, tests were previously carried out at different speeds between 150 and 200 mm/min, and it was concluded that the speed variation within this range has no influence on the measured stiffness. Deformation was obtained by Digital Image Correlation (DIC) [31,32] from images taken with a Nikon D5300 camera. The images were processed using Tracker software [33]. This technique also allows the detection of debonding or slippage of the adhesive relative to the clamps. Fig. 3 a) shows the experimental setup with the planar specimen, the clamps and the camera lens.

The stress-strain curves obtained in the different planar tests with specimens of different dimensions were analysed, and those showing the highest and lowest stiffness were selected for the study.

2.2. Traction uniaxial test

Uniaxial tensile tests were carried out on dumbbell specimens. Specimen dimensions are defined in ISO 37:2005. The dumbbell specimens were obtained using a die-cutting machine from a 3 mm thick adhesive sheet, previously cured and tested by the method described above. The halter specimens were tested using the same equipment previously used for the planar specimens, except for the grips, which were adapted to the dimensions of the new specimens. A test speed of 200 mm/min was set for the dumbbell specimen, also according to standard ISO 37:2005. Strain data were also obtained using the DIC technique.

2.3. Adjustment of hyperelastic models

For the comparison between the different applicable models and the estimation of the corresponding hyperelastic constants, the Abaqus software [27] has been used. The input data to the program are the nominal stress-nominal strain curves, from which the program estimates the constants of the different possible models by means of least squares.

The material models considered were Neo-Hookean, Mooney-Rivlin (polynomial N = 1) and Ogden (N = 1 and N = 2) [28,34,35]. It should be noted that in this case, the compressibility constants are zero for each

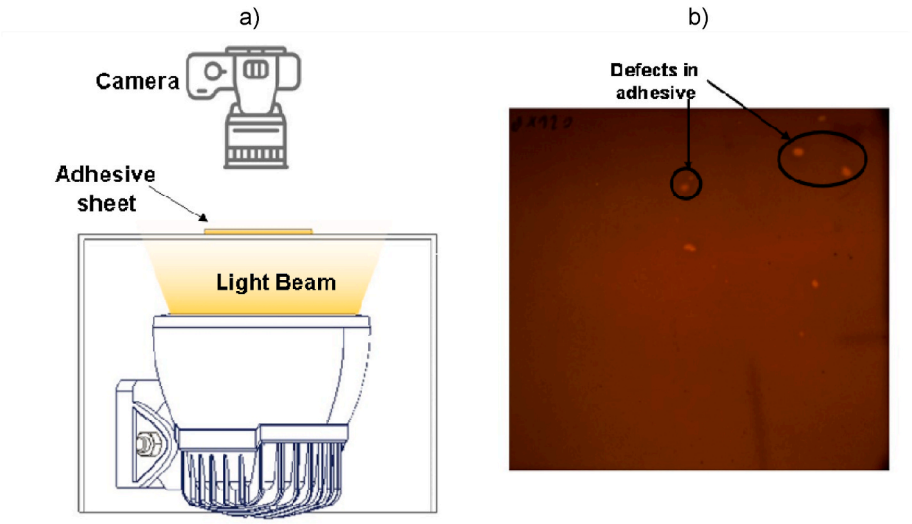

Fig. 2. a) Equipment for visual inspection by non-destructive testing; b) Adhesive film with defects.

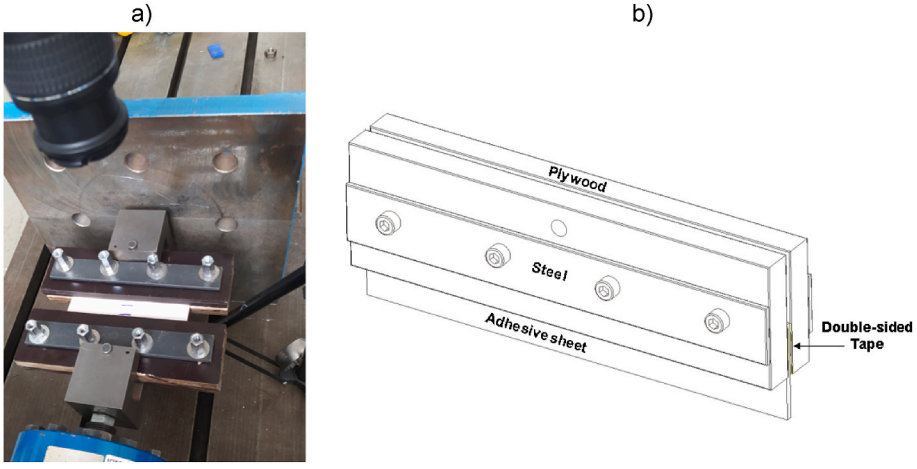

Fig. 3. a) Planar shear test equipment and specimen; b) Planar mounting clamps.

of the models, as the material is assumed to be incompressible.

In order to select the hyperelastic model that best reproduces the mechanical behaviour of the planar test and to determine the most appropriate specimen dimensions to obtain the hyperelastic constants, the curves obtained by simulation were compared with the stress-strain curves obtained in tests using CORA. The Correlation and Correlation Analysis (CORA) method is used in the validation of FEM models. Gehre et al. [36] first proposed the CORA method as an objective comparison technique to assess the level of agreement between two curves. The CORA method consists of four independent procedures to separately assess the size, phase, shape and corridor agreement of the two curves. Each procedure provides a score (ratio) between zero and one, where zero indicates no agreement between the signals and one indicates perfect agreement. This method of curve comparison has been used in many fields, particularly for the validation of non-linear numerical models [37,38].

2.4. Application and validation of hyperelastic models with SLJ specimens

The most common standards describing the production of SLJ specimens are ASTM D1002 and ISO 9664 [39]. This type of test generates only shear stresses and avoids uncontrolled deformation of the adhesive, thus preventing the occurrence of peel stress components. The specimens consist of two 100 mm long x 25 mm wide x 12 mm thick steel plates bonded together with SikaFlex 252 adhesive, with an overlap length of 25 mm and an adhesive thickness of 3 mm, as shown in Fig. 4 a). All specimens were prepared in a clean and stable environment (temperature 23 ± 3 °C; humidity 50 ± 5 %). The complete bonding process consists of three steps. First, the surfaces of the adhesives were degreased with acetone. Secondly, following the adhesive manufacturer's instructions, a primer was applied to the substrates, being from the same manufacturer as the adhesive, SikaPrimer 206. Finally, 1 h after applying the primer, the adhesive was applied to the substrate. The thickness of the adhesive was precisely adjusted using specific tooling, with a tolerance of 0.1 mm.

The specimens were cured in a controlled room at 23 ± 3 °C and 50 ± 5 % humidity for 15 days. The time of curing was previously stablished through a series of test on different curing-time SLJ specimens, finding that the stiffness obtained remained stable for periods longer than 15 days. It should be noted that as the adhesive thickness increases the curing time also should be increased. Therefore, following a similar process, the curing time was stablished in 35 days for the 6 mm thick specimens.

The steel plates are placed in the clamps of the testing machine, fixed by means of bolts and adjusting plates (Fig. 4 b). This rigid embedding ensures that the adhesive works in shear, and peeling stresses are negligible, despite the fact that the specimen is a single overlap specimen. Displacement is applied to the moving clamp at a speed of 10 mm/

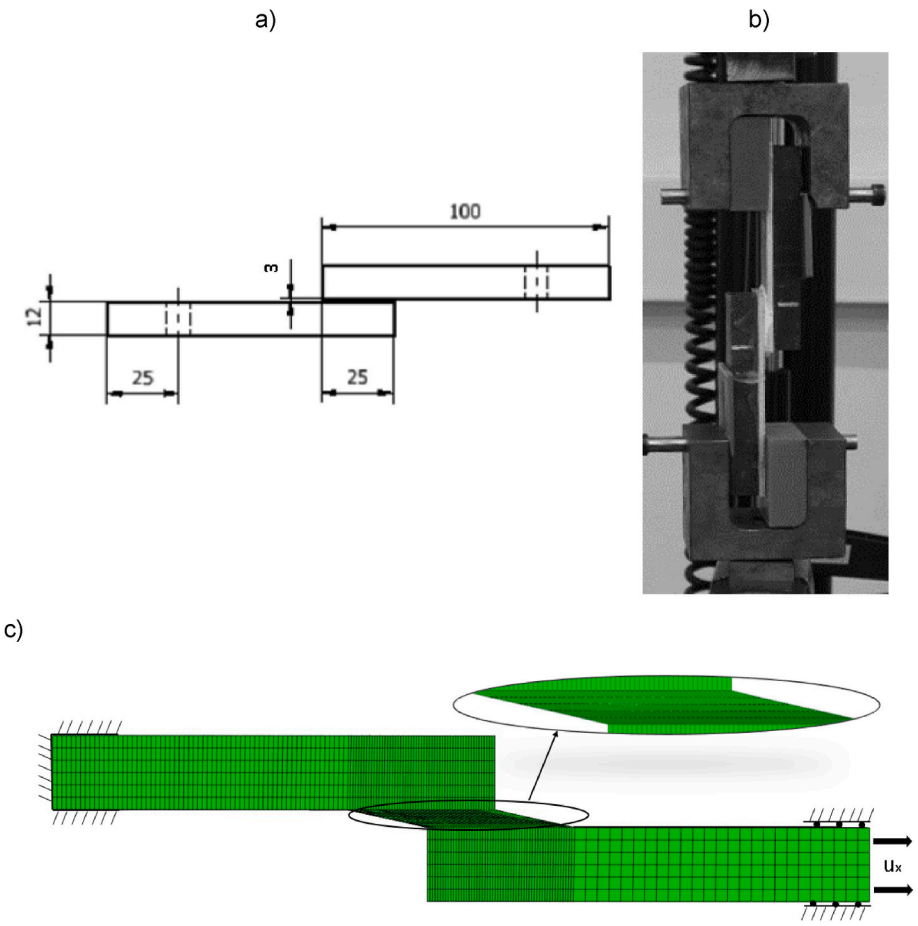

Fig. 4. a) SLJ specimen geometry (dimensions in mm); b) SLJ setup test; c) FE simulation SLJ.

min, according to others works in literature [40]. During the test, the clamp displacement and the force measured by the load cell are recorded, while temperature and humidity are maintained at controlled values (23 ± 3 °C; 50 ± 5 %).

In order to select, on the one hand, the optimum width of the planar specimen and, on the other hand, the grade of material that best fits the experimental results, the SLJ specimen with a thickness of 3 mm is modelled. The FEM model of the SLJ test is created in Abaqus. In this model, the results of the different hyperelastic models are compared using the constants obtained in the previous section from the combination of the dumbbell and planar specimens that showed the highest and lowest stiffness. Following a mesh convergence study, the element sizes for the SLJ specimen models were set at 2 mm for the steel plates and 0.6 mm for the adhesive. The element types used were hexahedral quadratic with reduced integration (C3D8RH). The boundary conditions were defined as shown in Fig. 4 c). The left end of the specimen is embedded, while a displacement (u_x) is applied at the right end to reproduce the test conditions.

As part of the validation of the adhesive characterisation, SLJ specimens are tested with three different adhesive thicknesses: 2, 4 and 6 mm, using the same configuration as for the 3 mm specimen. The aim is to evaluate the ability of the fitted model to predict the behaviour of the adhesive from one thickness to reproduce the behaviour of the material for bonds with other adhesive thicknesses.

3. Results and discussion

3.1. Tests with planar specimen

As can be seen from the stress-strain curves shown in Fig. 5, the

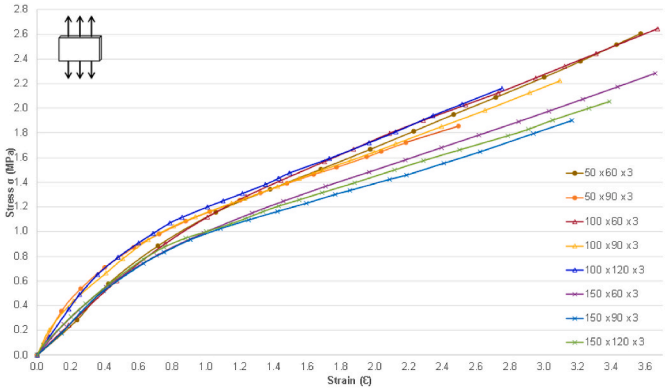

Fig. 5. Pure shear test results for the different dimensions of planar specimens.

stiffness is not significantly affected by the effective length of the specimen for the three widths considered. Nor is the stiffness affected by varying the specimen with a width between 50 and 100 mm. However, at a specimen width of 150 mm, a decrease in stiffness is observed. This is most clearly seen in Fig. 6, in which specimens of length 90 mm and widths 50, 100 and 150 mm are compared. In view of these results, tests were carried out by increasing the width of the specimen above 150 mm, maintaining a total length of 90 mm, obtaining a very similar stiffness to that obtained for the 150 mm specimen (the result for a 200 mm specimen is included in Fig. 6). It therefore appears that for widths greater than 150 mm, the stiffness value obtained is maintained. The same Fig. 6 also shows the results of a specimen of dimensions 150 × 90 mm and

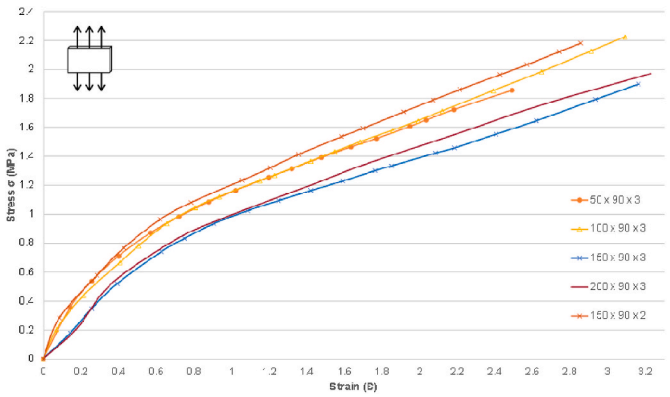

Fig. 6. Pure shear test results for total length 90 mm.

thickness 2 mm. This specimen shows a stress-strain curve of higher stiffness than its 3 mm equivalent.

In conclusion, there is a distinction between two groups of specimens. Specimens with a width of less than 150 mm have a higher stiffness. This may be due to the effect of the free edge of the adhesive film on the stresses, which has a greater weight on the narrow specimens. But once a sufficient width limit has been exceeded to eliminate this influence, increasing the width beyond 150 mm does not lead to a further decrease in stiffness.

On the other hand, the thickness of the adhesive film also influences the stiffness, even more than the width of the specimen. If the film thickness is too thin, the film will be too stiff and may be preventing the deformation in that direction necessary to assume a pure shear case.

After this analysis, it has been deduced that the planar specimen used for the characterisation of the hyperelastic material should be sufficiently wide and thick, and a priori the specimen with dimensions 150 × 90 × 3 mm could be the one selected for the fitting of the models.

However, in order to compare the results obtained in the characterisation and adjustment of the behavioural laws, the experimental data corresponding to the 100 × 120 × 3 mm specimen will also be used in the following section, as a representative of the group of planar specimens with the highest stiffness.

3.2. Model definition and estimation of hyperelastic constants

The curves obtained with the Neo-Hookean, Mooney-Rivlin and Ogden models are shown together with the validation curve in Figs. 7 and 8. At the beginning of the research, other models were also considered but rejected due to inaccurate fit. The analysis of these figures shows that the Ogden model with N = 2 and the Mooney-Rivlin model give the best fit to the experimental results, both for the dumbbell specimen and for the 150 × 90 mm planar configuration (the least

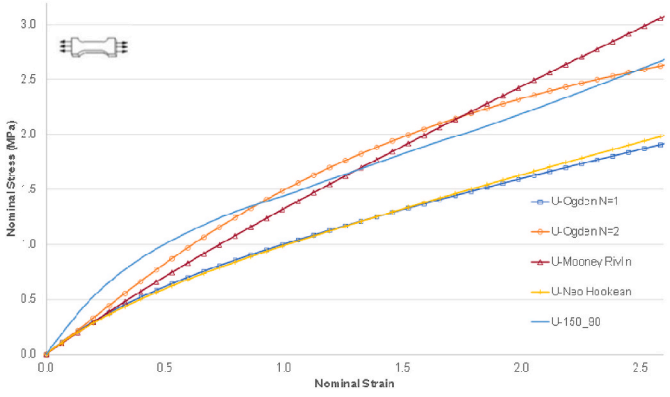

Fig. 7. Uniaxial test results for the considered models (150 × 90 × 3 mm).

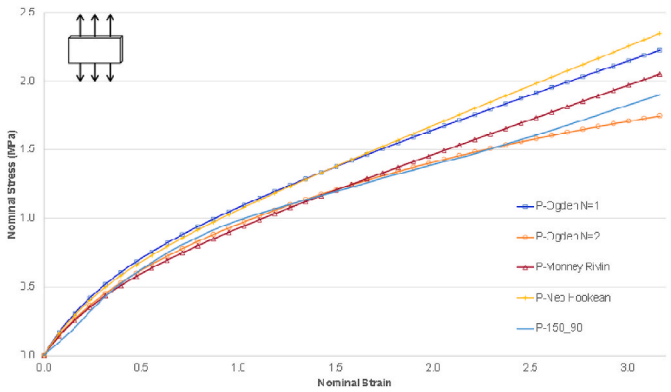

Fig. 8. Planar shear test results for the considered models (150 × 90 × 3 mm).

rigid). As can be seen in Table 2, the comparison of the curves with CORA shows that the hyperelastic model that best reproduces the experimental test is Ogden 2 (ratio = 0.908 for the uniaxial test, ratio = 0.962 for the planar test), followed by Mooney-Rivlin (ratio = 0.844 for the uniaxial test, ratio = 0.914 for the planar test). The hyperelastic constants for both models estimated from the 150 × 90 × 3 mm specimen are given in Table 3 and Table 4. The Ogden N = 1 and Neo-Hookean models deviate the most from the experimental curve, overestimating the stiffness in the uniaxial test and underestimating it in the planar test.

On the other hand, evaluating the curves obtained with the 100 × 120 × 3 mm (the most rigid) planar specimen configuration, the curves shown in Figs. 9 and 10 were obtained. The hyperelastic material model that most accurately matches the test curves is Ogden 2 (ratio = 0.899 for the uniaxial test, ratio = 0.933 for the planar test), followed again by the Mooney-Rivlin model (ratio = 0.811 for the uniaxial test, ratio = 0.836 for the planar test), see Table 5.

Estimated hyperelastic constants for the models from the 100 × 120 × 3 mm planar specimen are given in Tables 6 and 7.

It is worth mentioning that, as a general rule, a value of 0 has been obtained during the fitting process for the parameter related to the compressibility of the material (D_1). That indicates that the estimated material law corresponds to an incompressible material, which would be in line with the literature [41].

3.3. Planar probe selection

Fig. 11 shows the results of simulations for an adhesive thickness of 3 mm, using different material models, compared to the results of the SLJ test (four tests were carried out and showed high repeatability, only one representative test is shown in the graph for clarity). It can be clearly seen that the simulation using as material law the constants obtained for the Ogden model with N = 2 and Mooney-Rivlin from the planar specimen with a width of 100 mm lead to higher stiffness results than the experimental ones.

On the contrary, simulations of the SLJ-3 mm specimen with the laws obtained from the 150 mm wide planar specimen lead to stiffness values much closer to the experimental ones. By using the Ogden N = 2 model as the law of material, an acceptable correlation between the numerical

Table 2
CORA rating for different hyperelastic models fitted with 150 × 90 × 3 mm specimen planar test and uniaxial test with dumbbell specimen.

Model	R-Planar	R-Uniaxial
Ogden N = 1	0.771	0.637
Ogden N = 2	0.962	0.908
Mooney-Rivlin	0.914	0.844
Neo-Hookean	0.758	0.642

Table 3
Ogden N = 2 hyperelastic constants calculated with planar probe of dimensions 150 × 90 × 3 mm.

N	μ	α	D_1
1	26.1395538	0.333618395	0
2	−25.6260766	0.16447488	0

Table 4
Mooney-Rivlin hyperelastic constants calculated with planar probe of dimensions 150 × 90 × 3 mm.

N	C_{10}	C_{01}	D_1
1	0.508815827	−0.261630636	0

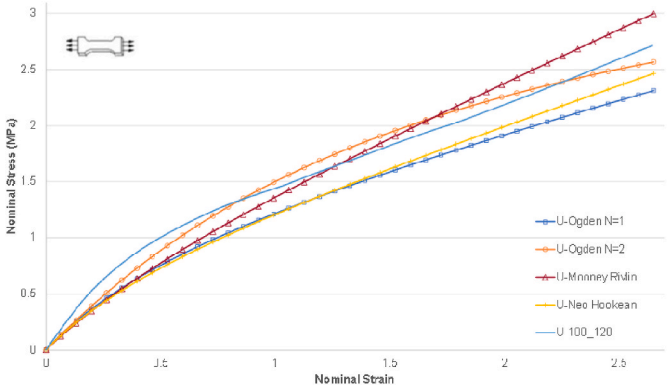

Fig. 9. Uniaxial test results for the considered models (100 × 120 × 3 mm).

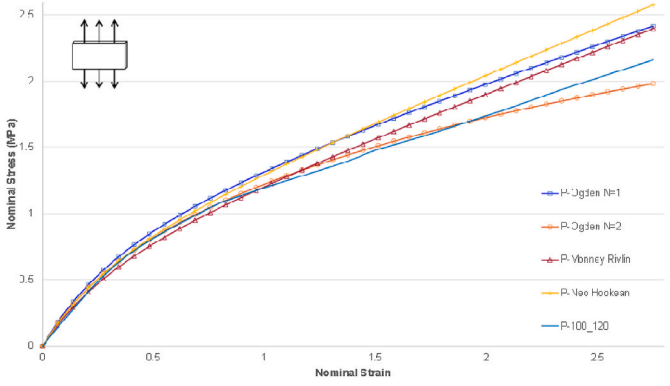

Fig. 10. Planar shear test results for the considered models (100 × 120 × 3 mm).

Table 5
CORA rating for different hyperelastic models fitted with 100 × 120 × 3 mm specimen planar test and uniaxial test with dumbbell specimen.

Model	R-Planar	R-Uniaxial
Ogden N = 1	0.747	0.686
Ogden N = 2	0.933	0.889
Mooney-Rivlin	0.836	0.811
Neo-Hookean	0.732	0.721

and experimental curve can be observed up to deformations of less than 10 mm. However, from this deformation onwards, a decrease in stiffness is observed in the simulation. However, the curves obtained using Mooney-Rivlin as the law of material showed an acceptable correlation with the test.

Table 6
Ogden N = 2 hyperelastic constants calculated with planar probe of dimensions 100 × 120 × 3 mm.

N	μ	α	D_1
1	4.32821536	0.736498262	0
2	−3.63425316	−0.06451675388	0

Table 7
Mooney-Rivlin hyperelastic constants calculated with planar probe of dimensions 100 × 120 × 3 mm.

N	C_{10}	C_{01}	D_1
1	0.456360914	0.135402423	0

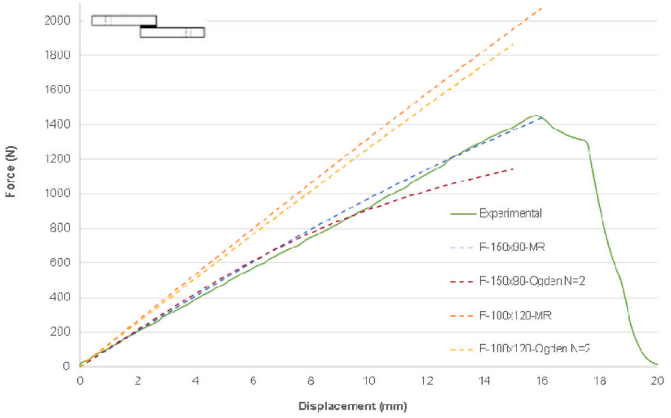

Fig. 11. Experimental and computational results for SLJ-3 mm. Comparison between the different models.

With these results, it can be said that the best material characterisation is obtained using the Mooney-Rivlin model, with the constants adjusted from the planar specimen of dimensions 150 × 90 × 3 mm.

However, the characterisation of the material could not be considered as completed, since the model has only been validated with 3 mm thick adhesive specimens. In the following section, these preliminary conclusions are validated by simulating tests on SLJ specimens of other thicknesses.

3.4. SLJ model validation

The Mooney-Rivlin hyperelastic model fitted from the 150 mm wide planar specimen was then used in FEM models of SLJ specimens with adhesive thicknesses of 2, 4 and 6 mm. The results obtained from the simulation show an acceptable correlation with the experimental results for all three specimen cases.

Looking in more detail at each of the test configurations, it can be seen in Fig. 12 that the slopes of the experimental and numerical curves are very similar in each of them. It can also be seen that the largest differences are close to half of the deformation for the 2 mm and 4 mm thick adhesive specimens.

In order to quantify the differences between the experimental and numerical curves, the relative error between the experimental and numerical curves was integrated over the deformation range in which the failure was not detected in the tests. The error with respect to the test results is shown in Table 8, which shows the average value of the relative error calculated with the different test curves available for each thickness. The largest error observed is 6 % for an adhesive thickness of 2 mm.

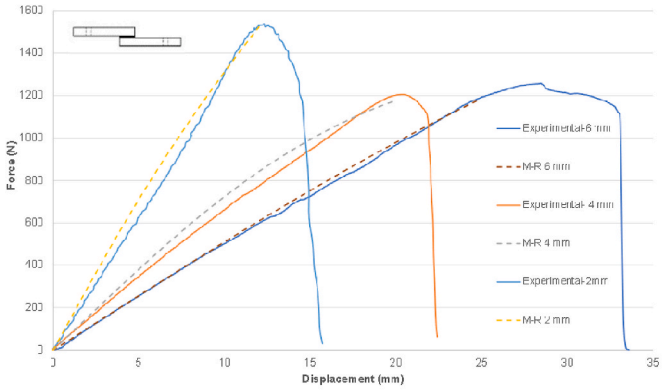

Fig. 12. Experimental results for SLJ-2-4-6 mm and computational result using Mooney-Rivlin (Model M-R).

Table 8
Relative error SLJ specimens.

SLJ	Relative error
2 mm	6 %
3 mm	2.4 %
4 mm	4.8 %
6 mm	2.1 %

4. Conclusions

In view of the results obtained, the objective of selecting and fitting a single hyperelastic model capable of reproducing the mechanical behaviour of a flexible adhesive with acceptable accuracy is considered to have been achieved. Starting from the results of two simple mechanical characterisation tests, uniaxial test and planar test, different hyperelastic models of the adhesive have been adjusted and then used in finite element modes to reproduce other types of tests, the results obtained by each of them have been compared, finally selecting the one that offers a sufficient level of accuracy.

The dimensions of the planar specimen from which the hyperelastic models are fitted have been found to influence the results. The width and thickness of the planar specimen were found to have a decisive influence on the results. And the minimum specimen width from which the data obtained from the pure shear test are considered valid for a good characterisation of the adhesive behaviour law has been determined.

Regarding the different hyperelastic models tested, the Ogden order 2 model and the Mooney-Rivlin model give very close results to the experimental ones when simulating the same specimens and test conditions used to fit the material models. However, when using these hyperelastic models to simulate the SLJ test, only the models fitted from testing planar specimens of sufficient width give acceptable results. The Mooney-Rivlin model is the one that has finally achieved the best fit, which seems to indicate that it is the most suitable to represent the behaviour of these adhesives.

It should be borne in mind, however, that the study was carried out on a single type of flexible polyurethane-based adhesive. In order to generalise the conclusions obtained, it will be necessary to validate the methodology defined in its application to other types of hyperelastic adhesives.

The results of this work will contribute to a better understanding of the behaviour of adhesives in different scenarios and working modes, and to the optimisation of simulation tools that allow the design of joints and the development of more efficient solutions adapted to different conditions of use.

Author statement

F.J. Simón-Portillo: Conceptualization, Methodology, Validation, Investigation, Writing - Original Draft, Writing - Review & Editing.

D. Abellán-López: Validation, Writing - Review & Editing, Methodology.

F. Arán-Ais: Resources, Investigation.

L.F.M. da Silva: Methodology, Supervision.

M. Sánchez-Lozano: Writing - Review & Editing, Supervision, Resources.

Declaration of competing interest

The authors declare that they have no known competing financial interests or personal relationships that could have appeared to influence the work reported in this paper.

Data availability

Data will be made available on request.

References

[1] J. Liu, T. Kan, J. Lou, L. Xiang, X. Zhu, Y. Tang, Localized damage response of carbon fiber reinforced polymer composite sandwich panel after thermal exposure, Polym. Test. 50 (2015), https://doi.org/10.1016/j.polymertesting.2015.12.006.

[2] S. Khalili, S.M.R. Khalili, R.E. Farsani, P. Mahajan, Flexural properties of sandwich composite panels with glass laminate aluminum reinforced epoxy facesheets strengthened by SMA wires, Polym. Test. 89 (2020), https://doi.org/10.1016/j.polymertesting.2020.106641.

[3] T.T.T. Nguyen, T.A. Le, Q.H. Tran, Composite sandwich structures in the marine applications, Sandw. Compos. Fabr. Charact. (Jan. 2022) 277–291, https://doi.org/10.1201/9781003143031-14.

[4] D. Gay, COMPOSITE MATERIALS: Design and Applications, THIRD EDITION, 2014, https://doi.org/10.1201/b17106.

[5] M.M. Sahib, G. Kovács, S. Szávai, Weight optimization of all-composite sandwich structures for automotive applications, Lect. Notes Mech. Eng. (2023) 720–733, https://doi.org/10.1007/978-3-031-15211-5_60.

[6] A. Tiwary, R. Kumar, J.S. Chohan, A Review on Characteristics of Composite and Advanced Materials Used for Aerospace Applications, 2021, https://doi.org/10.1016/j.matpr.2021.06.276.

[7] H. Chen, D. Wang, J. Na, X. Chen, Effect of sealing treatment on mechanical properties of CFRP-Aluminum alloy single lap joints, Int. J. Adhesion Adhes. 119 (Dec. 2022), 103236, https://doi.org/10.1016/J.IJADHADH.2022.103236.

[8] X. Xiong, et al., The effect of inclusions embedded in the adhesive on the stress distribution and strength of single-lap adhesive joints: analytical and numerical analysis, Int. J. Adhesion Adhes. 118 (Oct. 2022), 103235, https://doi.org/10.1016/J.IJADHADH.2022.103235.

[9] X. Shang, E.A.S. Marques, J.J.M. Machado, R.J.C. Carbas, D. Jiang, L.F.M. da Silva, Review on techniques to improve the strength of adhesive joints with composite adherends, Composites, Part B 177 (Nov. 2019), 107363, https://doi.org/10.1016/J.COMPOSITESB.2019.107363.

[10] A. Chiminelli, C. Valero, M. Lizaranzu, C.I. López, M. Canales, Modelling of bonded joints with flexible adhesives, J. Adhes. 95 (5–7) (Jun. 2019) 369–384, https://doi.org/10.1080/00218464.2018.1562347.

[11] R. M. Guedes, A. Sá, and M. F. S. F. De Moura, "Test Method an experimental and numerical assessment of DCB tests on glass/polyester curved beams cut out from pipes," Polym. Test., vol. 27, pp. 985–994, doi: 10.1016/j.polymertesting.2008.08.011..

[12] L.F.M. da Silva, R.D.S.G. Campilho, Advances in numerical modelling of adhesive joints, SpringerBriefs Appl. Sci. Technol. (2012) 1–93, https://doi.org/10.1007/978-3-642-23608-2_1/FIGURES/64, 9783642236075.

[13] C. Amstutz, M. Bürgi, P. Jousset, Characterisation and FE simulation of polyurethane elastic bonded joints under multiaxial loading conditions, Int. J. Adhesion Adhes. 83 (Jun. 2018) 103–115, https://doi.org/10.1016/J.IJADHADH.2018.02.029.

[14] B. Schaaf, M. Feldmann, Approach for the simulation of the load-deformation behaviour of hyperelastic bonded joints using strain and strain rate dependent tangent moduli, Int. J. Adhesion Adhes. 124 (May 2023), 103395, https://doi.org/10.1016/J.IJADHADH.2023.103395.

[15] M.D. Banea, L.F.M. da Silva, Mechanical characterization of flexible adhesives, J. Adhes. 85 (4–5) (2009) 261–285, https://doi.org/10.1080/00218460902881808.

[16] B. Burchardt, Advances in polyurethane structural adhesives, Adv. Struct. Adhes. Bond. (2010) 35–65, https://doi.org/10.1533/9781845698058.1.35.

[17] G.A. Holzapfel, Nonlinear Solid Mechanics : a Continuum Approach for Engineering, Wiley, 2000, p. 455.

[18] A.F. Bower, Applied Mechanics of Solids - Allan F. Bower - Google Libros, CRC press, 2009.

[19] M. Mooney, A theory of large elastic deformation, J. Appl. Phys. 11 (9) (1940) 582–592, https://doi.org/10.1063/1.1712836.
[20] K.K. Dwivedi, P. Lakhani, S. Kumar, N. Kumar, A hyperelastic model to capture the mechanical behaviour and histological aspects of the soft tissues, J. Mech. Behav. Biomed. Mater. 126 (Feb. 2022), 105013, https://doi.org/10.1016/J.JMBBM.2021.105013.
[21] R.W. Ogden, G. Saccomandi, I. Sgura, Fitting hyperelastic models to experimental data, Comput. Mech. 34 (6) (Aug. 2004) 484–502, https://doi.org/10.1007/S00466-004-0593-Y.
[22] A.F. Müller, et al., Evaluation of hyperelastic constitutive models applied to airway stents made by a 3D printer, IFMBE Proc 83 (2022) 881–889, https://doi.org/10.1007/978-3-030-70601-2_132.
[23] M.E. Çetin, Fabrication, Characterization and Mechanical Testing of Carbon Fiber Sandwich Composites with Nanoparticle Included Polyurethane Adhesives, vol. 56, Dec. 2021, pp. 589–603, https://doi.org/10.1177/00219983211058801, 4.
[24] H. Gründemann, R.W. Ogden, Non-linear elastic deformations. Ellis horwood ltd. 1984. Chichester, distributors: john wiley & sons ltd., XV, 532 S., £ 35.00. ISBN 0-85 312-273-3, ZAMM - J. Appl. Math. Mech./Z. Angew. Math. Mech. 65 (9) (Jan. 1985), https://doi.org/10.1002/ZAMM.19850650903, 404–404.
[2][5]] V. Dias, C. Odenbreit, O. Hechler, F. Scholzen, T. Ben Zineb, Development of a Constitutive Hyperelastic Material Law for Numerical Simulations of Adhesive Steel-Glass Connections Using Structural Silicone, 2013, https://doi.org/10.1016/j.ijadhadh.2013.09.043.
[26] J. Dispersyn, S. Hertelé, W. De Waele, J. Belis, Assessment of Hyperelastic Material Models for the Application of Adhesive Point-Fixings between Glass and Metal, 2017, https://doi.org/10.1016/j.ijadhadh.2017.03.017.
[27] Abaqus, Abaqus User Manual 6.14, Abaqus, 2020.
[28] L.E. Crocker, B.C. Duncan, R.G. Hughes, J.M. Urquhart, Hyperelastic Modelling of Flexible Adhesives, 1999, pp. 1–42. May. (Accessed 15 June 2021).
[29] D.C. Moreira, L.C.S. Nunes, Comparison of simple and pure shear for an incompressible isotropic hyperelastic material under large deformation, Polym. Test. 32 (2) (Apr. 2013) 240–248, 10.1016.
[30] M. Drass, J. Schneider, S. Kolling, Novel volumetric HELMHOLTZ free energy function accounting for isotropic cavitation at finite strains, Mater. Des. 138 (2018) 71–89, https://doi.org/10.1016/j.matdes.2017.10.059.
[31] Ukovich Walter, Digital Imaging Techniques in Experimental Stress Analysis, Optical engineering, 2019.
[32] H. Schreier, J.J. Orteu, M.A. Sutton, Image correlation for shape, motion and deformation measurements: basic concepts, theory and applications, Image Correl. Shape, Motion Deform. Meas. Basic Concepts,Theory Appl. (2009) 1–321, 10.1007/978-0-387-78747-3.
[33] Tracker video analysis and modeling tool for physics education. https://physlets.org/tracker/. (Accessed 26 July 2023).
[34] A. Dorfmann, K.N.G. Fuller, R.W. Ogden, Shear, compressive and dilatational response of rubberlike solids subject to cavitation damage, Int. J. Solid Struct. 39 (7) (Apr. 2002) 1845–1861, https://doi.org/10.1016/S0020-7683(02)00008-2.
[35] B Duncan, L. Crocker, "Characterisation of Flexible Adhesives for Design", doi: 10.47120/npl.mgpg45..
[36] C. Gehre, H. Gades, P. Wernicke, Objective rating of signals using test and simulation responses, in: Processding of 21st International Technical Conference on the Enhanced Safety of Vehicles Conference (ESV), 2009, pp. 15–18.
[37] S. Barbat, Y. Fu, Z. Zhan, C. Gehre, Objective rating metric for dynamic systems, Enhanc. Saf. Veh. (2013) 1–10.
[38] D. Abellán-López, M. Sánchez-Lozano, L. Martínez-Sáez, Frontal Crashworthiness Characterisation of a Vehicle Segment Using Curve Comparison Metrics, 2018, https://doi.org/10.1016/j.aap.2018.04.017.
[39] R.K. Behera, S.K. Parida, R.R. Das, Effect of using fibre reinforced epoxy adhesive on the strength of the adhesively bonded Single Lap Joints, Composites, Part B 248 (Jan. 2023), 110358, https://doi.org/10.1016/J.COMPOSITESB.2022.110358.
[40] P. Galvez, J. Abenojar, M.A. Martinez, Durability of Steel-CFRP Structural Adhesive Joints with Polyurethane Adhesives, 2018, https://doi.org/10.1016/j.compositesb.2018.11.097.
[41] Ali, A Review of constitutive models for rubber-like materials, Am. J. Eng. Appl. Sci. 3 (1) (Jan. 2010) 232–239, https://doi.org/10.3844/AJEASSP.2010.232.239.